Journal of Hazardous Materials 504 (2026) 141239

Contents lists available at ScienceDirect

Journal of Hazardous Materials

journal homepage: www.elsevier.com/locate/jhazmat

Toxicological and metabolomic assessment of the acute and sub-chronic effects of nanoceria (≤ 50 nm) on the human alveolar cells A549

Antonio Laganà [a,1], Barbara Billè [b,1], Angela Di Pietro [a], Alessio Facciolà [a], Consuelo Celesti [c], Daniela Iannazzo [c], Mariachiara Galati [b], Maria Maisano [b,d], Tiziana Cappello [b,d,e,2,*], Giuseppa Visalli [a,2]

[a] Department of Biomedical and Dental Sciences and Morphofunctional Imaging, University of Messina, Messina 98125, Italy
[b] Department of Chemical, Biological, Pharmaceutical and Environmental Sciences, University of Messina, Messina 98166, Italy
[c] Department of Electronic Engineering, Industrial Chemistry and Engineering, University of Messina, Messina 98125, Italy
[d] University Centre for the Protection and Management of Natural Environments and Agro-Ecosystems (CUTGANA), Catania 95123, Italy
[e] Universal Scientific Education and Research Network (USERN), Italy

HIGHLIGHTS

- The impact of nanoceria was comprehensively tested on human alveolar A549 cells
- Dose- and time-dependent cytotoxicity, oxidative stress, and mitochondrial damage occurred
- Metabolomics revealed alterations in energy, redox, and membrane-related pathways
- Sub-toxic exposure induced adaptive responses, while toxic doses caused irreversible effects

GRAPHICAL ABSTRACT

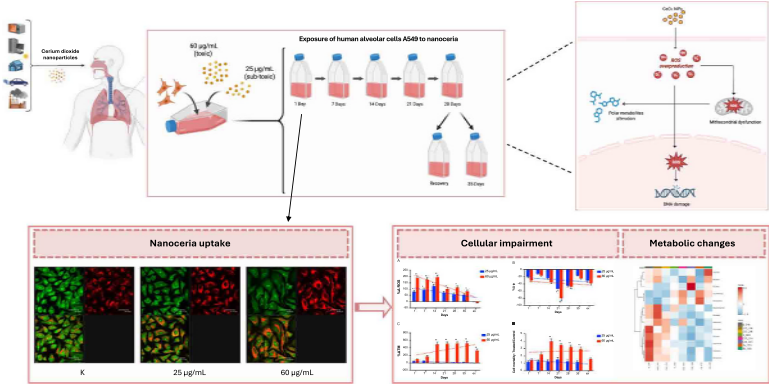

ARTICLE INFO

Keywords:
Cell progeny
Mitochondrial impairment
DNA damage
^{1}H NMR metabolomics
Homeostatic mechanisms

ABSTRACT

In a society focused on sustainability, green technologies expand the use of Rare Earth Elements (REEs). Cerium dioxide nanoparticles (CeO_2NPs) possess redox/catalytic activity but raise inhalation concerns. We evaluated their effects in alveolar A549 cells exposed to 25 and 60 µg/mL, equal to 37 % and 89 % of the IC50, respectively. Acute exposure was evaluated at 24 h, whereas sub-chronic exposure spanned 35 days, besides recovery was assessed in cell progeny grown in CeO_2NPs absence. A multiparametric strategy combined MTT viability, ROS, mitochondrial membrane potential (ΔΨm), DNA damage (Comet assay), cell replication index (WCRI), and untargeted ^{1}H NMR metabolomics. MTT showed dose-dependent cytotoxicity (IC_{50}=67.7 µg/mL). Both

* Correspondence to: Department of Chemical, Biological, Pharmaceutical and Environmental Sciences, University of Messina, Viale F. Stagno d'Alcontres 31, Messina 98166, Italy.
E-mail address: tcappello@unime.it (T. Cappello).
[1] These authors contributed equally to this work.
[2] These authors share last authorship

https://doi.org/10.1016/j.jhazmat.2026.141239
Received 19 October 2025; Received in revised form 24 December 2025; Accepted 22 January 2026
Available online 24 January 2026

concentrations increased ROS and decreased ΔΨm, with partial recovery only at 25 μg/mL. DNA damage was negligible at 25 μg/mL but persisted at 60 μg/mL during sub-chronic exposure, whereas WCRI declined with dose. Metabolomics indicated adaptive responses at 25 μg/mL (elevated glycolytic/TCA/redox metabolites), and depletion in metabolite levels at 60 μg/mL, consistent with early mitochondrial dysfunction. After 35 days of exposure, both doses caused reduction of glycine, cysteine, serotonin, acetylcholine, betaine, glucose, and succinate, and accumulation of lactate, malonate, and glutamine, indicating Warburg shift and TCA disruption. Glutathione exhibited a biphasic response. Recovery of metabolism and function occurred only at the sub-toxic dose. Overall, CeO_2NPs trigger concentration- and time-dependent cytotoxic, oxidative, mitochondrial, genotoxic, and metabolic alterations in A549 cells. These mechanistic findings support the dual antioxidant/pro-oxidant role of nanoceria and its classification as an emerging inhalable pollutant of concern for human health.

1. Introduction

In a society increasingly focused on the sustainability, green technologies are gaining ground, becoming the emerging technologies par excellence. These require massive use of the so-called Rare Earths Elements (REEs), particularly needed in the production of clean energy production such as wind turbines, solar panels, and electric vehicles [1]. Although REEs are widespread in the Earth's crust, mainly in the form of oxides, their mobilization could have a significant impact on both ecosystems and human health [2] due to their metallic nature, which allows them, once released, to remain permanently in the environment. Therefore, REEs have been suggested as contaminants of emerging concern worldwide [3–6].

Among these elements, also referred to as lanthanides, cerium (atomic number 58) is abundantly present, in particular as dioxide (CeO_2). This compound, able to self-assemble as crystalline nanoparticles (CeO_2NPs) and more commonly referred to as nanoceria, is to be considered a metal-based nanomaterial that can be used as it is or further engineered through functionalisation [7]. Similarly to all nanomaterials, the extremely small dimensions confer specific properties to CeO_2NPs that are absent in the bulk material [8,9]. This is attributable to the nanoscale size which, by significantly increasing the surface area, makes the nanoparticles extremely reactive per unit of mass [10].

Thanks to its peculiar features, including its marked catalytic properties, nanoceria is increasingly used in a variety of applications both in industry and in the manufacturing of several products, such as chemical mechanical polishing for optical elements, planarization for semiconductor wafers, UV-shielding, solar cells, toner, fuel additives, fuel cells, electrochemical devices for everyday use, automotive catalytic converters (ACCs), diesel particulate filters (DPFs), production of nanocomposites, etc. With an annual global production equal to 68,500 tonnes in 2019, CeO_2 is the most used oxide of the lanthanides [11].

The occupational exposure is therefore not negligible, while an unintentional exposure of individuals, previously solely due to CeO_2 use as a fuel additive in diesel engines, is believed to increase significantly in the near future. This will also be caused by the disposal into the environment of the various devices in which the compound is used, making the potential negative effects attributable to the overtime nanoceria release into the environment no longer negligible.

The increased cerium use in emerging technologies is due to its electronic configuration. It exhibits the ability to be oxidised and reduced very rapidly and efficiently (redox behaviour), and the changes of the oxidation state between Ce^{3+} and Ce^{4+} give it exceptional catalytic and enzyme-like characteristics. While the oxido-reduction cycle makes nanoceria powerful scavengers of reactive oxygen species (ROS), the dual role of Ce^{3+} should be considered. Analogously to transition metals, in H_2O_2 presence, Ce^{3+} has a powerful pro-oxidant effect by catalysing the production of °OH in Fenton/Haber Weiss reactions [12]. The redox changes, occurring exclusively on the particle surfaces, are inversely related to size and are due to Ce^{3+}/Ce^{4+}, which in turn is regulated by the nanoceria production process, during which O vacancies are formed, modifying the nanoceria redox behaviour [8].

Furthermore, similarly to all nano-sized particles, both natural and released into the environment as a result of anthropic activities, nanoceria can easily cross biological membranes and internalise into organisms, including humans [3,4,13,14–16]. This makes it of fundamental importance to evaluate its biological effects.

Depending on all the above-reported variables, the data present in the literature are extremely discordant and, in addition to a powerful free radical scavenging effect observed by some [17–19], others instead underlined a significant pro-oxidant effect of nanoceria, as reported in the comprehensive review of Yokel et al. [20], to which we refer. Considering that the redox imbalance is at the root of the pathogenesis of nearly all non-communicable diseases (NCD), the scavenging function of nanonoceria is particularly intriguing and has drawn the attention of several researchers for potential medical applications, also by resorting to doped nanoceria [7,21]. However, even aside from medical use, the toxicological characterisation of nanoceria is essential, particularly in light of toxicokinetic studies demonstrating that only trace amounts of nanoceria are eliminated in urine and faeces following intravenous treatment [22].

Therefore, we performed an *in vitro* study by exposing a human alveolar cell line to CeO_2NPs. Considering that both occupational and unintentional exposure to environmental pollution are prolonged over time, in addition to short-term effects, we assessed the impact of the sub-chronic exposure. To this aim, we simulated the actual exposure conditions, extending the nanoceria treatment up to 35 days in subsequent subcultures of the exposed cells and, in order to assess the ability of the cell progeny to restore basal conditions, our experiments were also performed in subcultures obtained from cells sub-chronically exposed but grown in its absence for a week.

In addition to classical toxicological endpoints such as cell viability, oxidative stress and mitochondrial function, we also investigated the intracellular metabolomic profile of exposed cells. Metabolomics is a rapidly expanding area of "omics" science focused on the accurate detection and characterization of low molecular weight metabolites [23]. In toxicological research, it provides a valuable tool to explore early biochemical perturbations, uncover potential mechanisms of toxicity, and identify relevant biomarkers associated with exposure to environmental contaminants [13,14,24–26]. By analysing the levels of key metabolites involved in redox balance, energy production, and membrane turnover, we aimed to better characterize the cellular response to nanoceria exposure and identify potential metabolic signatures associated with both reversible and persistent damage, as well as to elucidate the mechanisms underlying long-term metabolic adaptation and cellular reprogramming.

2. Materials and methods

2.1. Exposure conditions and cell models

A commercial cerium oxide nano-powder (CeO_2NP) that had a median primary particle diameter of 50 nm (Sigma-Merck, n° code 700290; Milan, Italy) was used starting from a stock suspension (10 mg/mL) in phosphate buffered solution (PBS). The working suspensions were freshly prepared in the cell medium and submitted to sonication to prevent particle aggregation. To characterize these working

suspensions, hydrodynamic diameter measurements and ζ-potential were detected by dynamic light-scattering (DLS) analyses using the Zetasizer 3000 instrument (Malvern, Worcestershire, UK), equipped with a 632 nm HeNe laser, operating at a 173-degree detector angle [27].

The A549 epithelial cell line (ATCC CCL-185 ™) was used since it is the model of choice for *in vitro* studies of airborne pollutants. The cells were cultured in F-12K medium (Gibco™ 21127022) supplemented with 2 mM of L-glutamine, 10 % of inactivated fetal bovine serum (FBS), and 1 % penicillin/streptomycin/amphotericin. The cells were grown in monolayer at 37 °C in a 5 % CO_2/95 % air humidified atmosphere and subcultured on a regular basis (usually every 4 days). Experiments were performed by exposing cell monolayers to CeO_2NP for the time and doses specified in the experimental protocol. In particular, for the assessment of short-term effects, the cells were exposed for 24 h. Sub-chronic exposure was performed by starting from the cells CeO_2NP treated for 24 h and subculturing $2 \times 104/cm^2$ cells in fresh nanoceria suspension added to growth media. Weekly, always using the same number of cells, subcultures were set up by using fresh CeO_2NP suspensions in growth medium. The procedure was repeated for 5 consecutive weeks, using the remaining aliquot of cells to assess the effects of exposure at 7, 14, 21, 28, and 35 days. In order to enable nearly continuous exposure of the cells to the specified nanoceria dosages, twice a week the nanoceria suspension in growth medium was replaced with a fresh suspension, subsequent to rinsing the monolayers with PBS to eliminate any residual CeO_2NPs. In parallel, the same experimental protocol was used for the control cells in which the CeO_2NP stock suspension was replaced by PBS. Based on this, the experimental design involved examining CeO_2NP-induced effects on five sequential cell progenies, each derived from the preceding progeny. Further experiments were performed on the subcultures obtained by cell progenies treated for 28 days. In particular for these experiments, two subcultures were performed, one of which was incubated for 7 days in growth media without nanoceria suspension, in order to assess the ability of the progeny, obtained from cells sub-chronically exposed to the xenobiotic, to restore basal conditions. All experiments were performed in triplicate.

2.2. Cytotoxicity assays and uptake assessment

Preliminarily, acute cytotoxicity of CeO_2NPs was evaluated in the range of 1.65–200 μg/mL through the colorimetric MTT assay that is based on the reduction of 3-(4,5-dimethiazol-2)-2,5-difeniltetrazolium bromide, catalysed by cellular dehydrogenase. Briefly, after verifying the absence of particle interference in the spectrophotometric detection through abiotic tests, the assay was performed in cells cultured for 24 h in 96-well microplates. The appropriate volume of the stock suspension of CeO_2NPs (10 mg/mL) was added to the cell medium (100 μL/well). After 24 h, using our standard protocol [28], the enzymatic activity of viable cells was quantified by spectrophotometric measurement at 540 nm using a microplate reader (Tecan Italia; Milan, Italy). Dimethyl sulfoxide (DMSO, 10 %) and PBS were used as positive and negative control, respectively.

To evaluate CeO_2NP uptake, the endocytic apparatus (late endosomes and lysosomes) was examined using the metachromatic fluorochrome Acridine Orange (AO). The red fluorescence emitted by AO in the acidic compartment, contrasted with the green fluorescence in the cytosol and nucleus, allows the red/green ratio to reflect both the uptake of exogenous material and the diminished cytoplasmic green fluorescence, indicative of acidic compartment leakage [29]. The investigations were conducted on semi-confluent A549 monolayers grown on chamber slides and treated for 2 and 5 h with CeO_2NP suspensions at concentrations of 25 and 60 μg/mL. Subsequent to the elimination of the medium and multiple washes with PBS, an AO solution (5 μg/mL) was added, and Confocal Laser Scanning Microscopy (CLSM) observations were performed using the Leica TCS SP2 apparatus (Leica Microsystems, Wetzlar, Germany), alongside Leica Confocal software (version 2.0) and the Leica DM IRB fluorescence microscope. The image-processing program Image (imagej.nih.gov/ij/index.html, accessed on 30 January 2025) was utilized to quantify the acid compartment by assessing the cellular area displaying red fluorescence and its intensity. A minimum of 100 cells was analyzed for each slide. Cells exposed to CeO_2-free medium served as negative controls. The percentage change (%Δ) in the product of area and emission intensity relative to negative controls was calculated.

2.3. Assessment of ROS production after acute and sub-chronic exposure and detection of ROS-induced effects

To assess the acute and sub-chronic effect, all tests were performed on cell aliquots treated with 25 and 60 μg/mL of CeO_2NPs for the times foreseen by the experimental protocol. It is important to note that all experiments were performed on live cells (i.e., adherent cells), whereas all supernatants were gathered to evaluate the percentage of dead cells.

ROS were measured by using the 2',7'-dichlorofluorescein-diacetate (DCF-DA) probe (Merck Life Science S.r.l.; Milan, Italy). Briefly, after repeated washing with PBS, cell suspensions were loaded with the probe solution (1 μM) prepared in PBS containing 10 mM of D-glucose (pH 7.4) and, after incubation at 37 °C for 30 min, the fluorometric readings were carried out at the excitation and emission wavelengths of 485 and 535 nm. For all spectrofluometric measurements, a microplate reader (Tecan; Milan, Italy) was used, and results were expressed as % change (%Δ) in comparison to control cells.

CeO_2NP-induced mitochondrial impairment was detected by the fluorescent probe rhodamine 123 (R123) (Invitrogen Molecular Probes; Eugene, OR, USA). This cationic fluorochrome measures transmembrane potential (ΔΨm) since it is stored only in the matrix of functional mitochondria where an active proton gradient is preserved during oxidative phosphorylation. The probe solution (10 μM final concentration) was added to the aliquots of control and treated cell suspensions, that were incubated for 10 min at 37 °C. After washing with PBS, fluorimetric readings were carried out using 535 and 595 nm as the excitation and emission wavelengths, respectively.

DNA damage induced by CeO_2NP exposure was evaluated in control and treated cells by using the alkaline version of the Comet assay. Tests were performed in duplicate, using 2×104 cells for each spot, and the electrophoresis was run for 30 min at 25 V and 300 mA (0.86 V/cm). The samples were stained with ethidium bromide (20 μg/mL) and imaged using a DMIRB fluorescence microscope (Leica Microsystems), equipped with a digital camera (Power Shot S50, Canon; Milan, Italy) at 400X total magnification. The Comet Assay Project (CASP) (http://ww25.casplab.com/?subid1=20230810–1122-084e-8a7d-57f935e2 83f5) program was used to evaluate the images of 100 cells per slide that were randomly obtained. The Tail Moment (TM) was used as the metric for assessing DNA damage.

The cytotoxicity, triggered by sub-chronic exposure to nanoceria, was evaluated by fluorimetric detection of cells detached from monolayers by using propidium iodide (PI) as probe. These, present in the supernatant, were incubated with PI solution (3 μg/mL) at 4 °C for 5 min, then the fluorescence of dead cells was measured using 535 and 615 nm as the excitation and emission wavelengths, respectively. By cell count, the weekly cell replication index (WCRI) was also evaluated.

2.4. Metabolomic analysis

2.4.1. Extraction of cellular metabolites

For proton Nuclear Magnetic Resonance (^{1}H NMR)-based metabolomic analysis, cells exposed to both concentrations of CeO_2NPs for 24 h and 35 days, and those incubated for 7 days without nanoceria after sub-chronic exposure were evaluated. For each time point, three independent biological replicates were performed, and each sample was analyzed in duplicate technical runs. The entire pellet obtained from treated and untreated A549 cells, grown in T25 culture flasks, was used

for metabolomic extraction.

Intracellular polar metabolites were extracted using a biphasic methanol/chloroform/water protocol adapted from previously validated methods [14,26]. Briefly, metabolic activity was quenched by adding 650 μL of cold 80 % methanol directly to the culture flasks. Cells were scraped, transferred to microcentrifuge tubes containing 0.5 mm glass beads, and vortexed for 1 min to promote mechanical lysis. Subsequently, 260 μL of chloroform was added, followed by an additional 260 μL of chloroform and 220 μL of water. Each step was followed by vortex mixing and samples were incubated on ice for 10 min. Phase separation was achieved by centrifugation at 2000 × g for 15 min at 4 °C. The upper aqueous phase (~400 μL), containing the hydrophilic metabolites, was carefully collected, dried using a centrifugal vacuum concentrator (Eppendorf 5301), and then stored at −80 °C. Prior to NMR analysis, the dried intracellular extracts were reconstituted in 600 μL of 0.1 M sodium phosphate buffer (pH 7.0) containing 10 % D_2O and 1 mM 2,2-dimethyl-2-silapentane-5-sulfonate (DSS; Sigma-Aldrich), and transferred into 5 mm NMR tubes for spectral acquisition.

2.4.2. ^1H NMR metabolomics and spectral pre-processing

The polar intracellular extracts were analysed by ^1H NMR spectroscopy using a Varian-500 spectrometer (499.74 MHz, 298 K). One-dimensional ^1H NMR spectra were acquired at 25 °C using a NOESY-presaturation (noesypr1d) sequence to suppress the water signal, with a 120 ms mixing time, 2 s relaxation delay, 256 transients, 11.68 ppm spectral width, and 32,768 data points with digital quadrature detection. Spectral processing included 0.5 Hz line broadening, Fourier transformation, manual phase and baseline correction, as well as chemical shift calibration to DSS (0.00 ppm), all performed using Chenomx Processor v12.0 (Chenomx Inc., Canada). Metabolites were identified via chemical shifts, signal multiplicity, and comparison to the Chenomx 500 MHz library and public databases. Quantification was performed using DSS as the internal reference standard [30–35].

2.4.3. Pathway enrichment and network analyses

To support the biological interpretation of the metabolomic profile alterations observed in nanoceria-exposed A549 cells, a functional metabolic analysis was performed using MetaboAnalyst 6.0 (https://www.metaboanalyst.ca) [36]. Lists of significantly altered intracellular metabolites ($p < 0.05$, ANOVA with Dunnett's post-test vs. control) were uploaded after ^1H NMR quantification, and annotated using the Human Metabolome Database (HMDB) identifiers.

For the pathway enrichment analysis, the Small Molecule Pathway Database (SMPDB) library (99 metabolite sets based on normal human metabolic pathways) was selected. Over-representation analysis (ORA) was carried out using the hypergeometric test with false discovery rate (FDR) correction. Pathways were ranked by statistical significance ($-\log_{10}$ p-value) and enrichment ratio.

For the pathway topology and network analysis, the Kyoto Encyclopedia of Genes and Genomes (KEGG) *Homo sapiens* pathway library was employed. Topology analysis was based on node centrality (degree and betweenness), integrating enrichment with pathway connectivity. A significance threshold of $p < 0.05$ (FDR-corrected) was applied. Results were visualized as dot plots (enrichment) and network graphs (topology), where node size indicates enrichment ratio and node colour corresponds to statistical significance.

2.5. Statistical analyses

All data are presented as mean ± standard deviation (SD) based on at least three independent experiments. Analyses were performed using the software GraphPad Prism (version 10). The relationships between different parameters were assessed by using the Pearson correlation coefficient, while the Student's *t*-test was used to assess the differences between samples. ANOVA was used to statistically analyze the NMR data, and the Dunnett's post-test was then used to assess changes among each treatment groups in relation to the control group. Pathway enrichment and network analyses were carried out in MetaboAnalyst 6.0, using over-representation analysis (hypergeometric test with FDR correction) for SMPDB pathways and topology-based analysis for KEGG pathways. Additionally, a correlation matrix in the form of a heatmap was constructed using MetaboAnalyst to highlight the variation in metabolite concentrations across samples and experimental conditions. Principal Component Analysis (PCA) was also performed in MetaboAnalyst 6.0 after log-transformation and Pareto scaling of metabolomic data to evaluate global variance structure and clustering patterns across exposure groups. Significance was accepted at $p < 0.05$.

3. Results

3.1. CeO2NP characterization

The analyses performed to test the colloidal stability of CeO_2NP in PBS and cell culture medium enabled us to investigate the influence of concentration and the biological environment on the surface charge and size distribution of the particles. At physiological pH and osmotic pressure, the zeta potential test revealed no surface charges on the particles. This resulted in a pronounced tendency for the particles to aggregate, simultaneously highlighting their significant hydrophobicity and, hence, their enhanced capacity to interact with biological membranes. Dimensional analysis at doses of 25 and 60 μg/mL validated aggregation, especially in cell culture medium, notwithstanding the pronounced colloidal instability of the suspensions, confirmed by the PI, always approximately equal to 1.00. In PBS, the DLS spectra indicated the existence of nanoaggregates with average diameters of 116.6 nm only at a concentration of 60 μg/mL. Instead, at a concentration of 25 μg/mL, the average diameter of 64.2 was somewhat greater than the manufacturer's certification (Figure S1 in Supplementary Materials). The tendency toward aggregation was more pronounced in the cell medium, distinguished by the presence of nutrients, including complex ones, such as FBS (10 % in growth medium). In this condition at the same doses of CeO_2NP, the spectra revealed the presence of peaks at 390.2 and 779.6 nm respectively (Figure S1 in Supplementary Materials).

3.2. CeO2NP cytotoxicity and uptake

To assess the acute cytotoxic effect of nanoceria, MTT test was performed on monolayers of A549 cell lines at 24 h. The assayed doses ranged from 1.65 to 200 μg/mL. CeO_2NP suspension had a moderate cytotoxicity (Figure S2 in Supplementary Materials), which was positively related to the exposure dose ($r = 0.887$, $p < 0.05$). The IC50 value of CeO_2NP was 67.69 μg/mL.

Based on the cytotoxic data, for the assessment of acute and subchronic effects of CeO_2NPs, two doses, termed as sub- and toxic dose, were selected. These doses were 25 and 60 μg/mL, equal to 37 % and 89 % of the IC50, respectively, chosen in order to assess the homeostatic capabilities of the selected cell model, highlighting a possible adaptation of the cellular progeny.

The uptake of CeO_2NP by A549 cells was assessed analysing the endocytic compartment by the metachromatic fluorophore AO. The results of confocal microscopy observations (Fig. 1) distinctly demonstrated a very fast internalization of nanoceria in mature endosomes. Following just two hours of treatment, a notable dose-dependent increase of the endocytic compartment was recorded and %Δ values were 30.1 and 50.9 for sub- and toxic doses, respectively ($p < 0.05$). A subsequent light increase (i.e., a bigger cell surface emitting in red) was noted exclusively at sub-toxic doses. Instead, at toxic doses, a significant reduction in the endocytic compartment was observed at 5 h ($p < 0.01$). Concurrently, a decrease in green emission was noted in these cells (%Δ–16), signifying a partial cytoplasmic acidification due to disruption of the phagolysosomal membranes, resulting in leakage of the engulfed

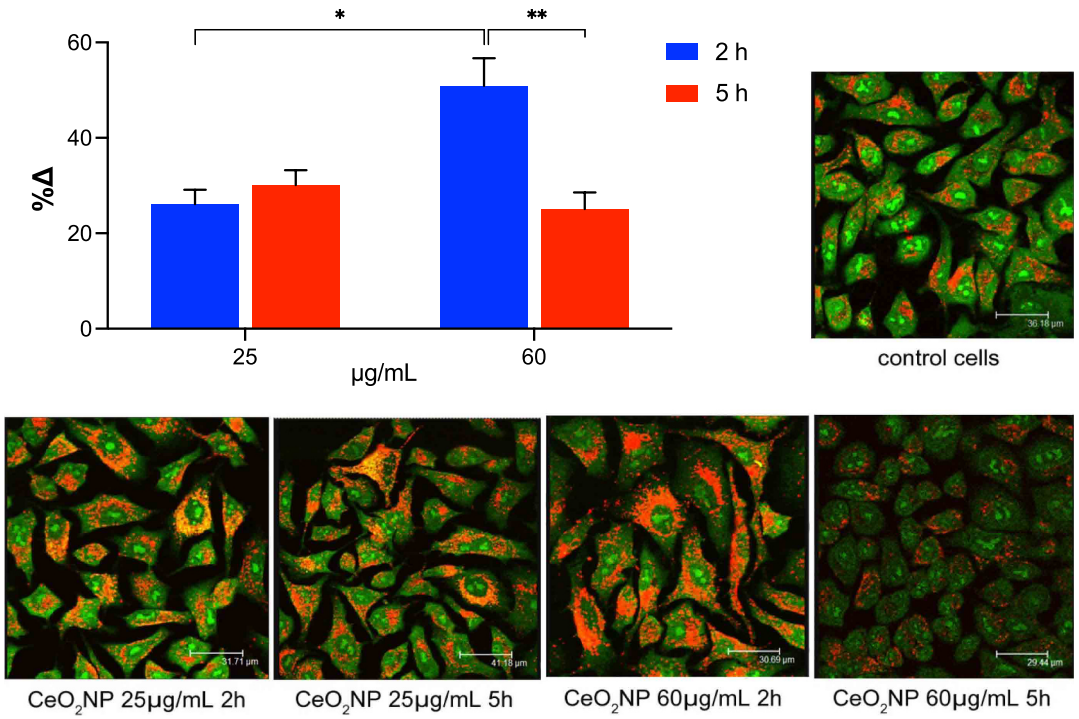

Fig. 1. Results of CLSM analyses with representative images of treated and untreated A549 cells by employing AO to evaluate the endocytic apparatus (red emitted fluorescence) and other cellular compartments (green emitted fluorescence). After treatment for 2 and 5 h with CeO_2NP (25 and 60 µg/mL), the acid compartment was quantified by assessing the cellular area displaying red fluorescence and its intensity. A minimum of 100 cells was analyzed for each slide. In the graph the average (± SD) of %Δ in comparison to control cells is reported (* $p < 0.05$; ** $p < 0.01$).

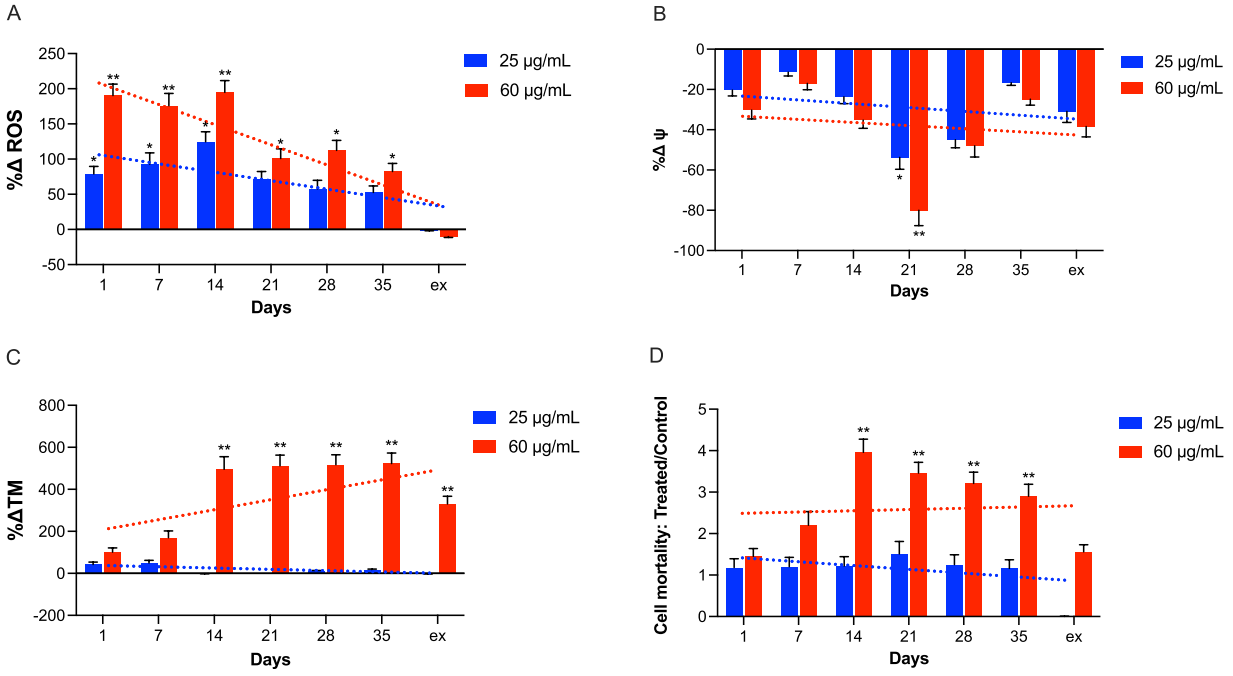

Fig. 2. Biological effects of acute and sub-chronic exposure to sub-toxic and toxic doses of CeO_2NPs. (A) The pro-oxidant effect of the xenobiotic was assessed by measuring ROS levels. The percentage changes (%Δ) were dose-dependent, and a significant ROS overproduction at the two doses was observed. (B) Evaluation of mitochondrial impairment by detecting transmembrane potential (ΔΨm). The %Δ values underline the dose dependent mitochondrial dysfunction, which even in the absence of exposure to the xenobiotic for seven days persisted in cell progeny. (C) Results of Comet assay, used for the assessment of CeO_2NP-induced DNA damage. The values, expressed as %Δ of Tail Moment (TM) and adjusted for cell mortality, highlight the distinct pattern between the two nanoceria doses. (D) Spectrofluorimetric detection of cell mortality, measured by the probe PI in the cell detached from monolayers. The values, expressed as Treated/Control ratio highlight the irreversible damage in cell progeny induced by the higher dose assayed (* $p < 0.05$; ** $p < 0.01$).

material.

3.3. Acute and sub-chronic effects of nanoceria

The pro-oxidant effect of nanoceria exposure is reported in Fig. 2A. ROS levels, expressed as percentage change (%Δ) were dose-dependent, and a significant ROS overproduction ($p = 0.045$ and 0.009 at the two doses, respectively) was observed. Compared to the levels recorded at 24 h (%Δ = 79.0 and 190.4 for the lower and higher doses, respectively), for both the tested doses a partial adaptation of the cellular progeny was observed starting from the 14th day. In particular, while in the first two weeks the cell progeny exposed to the toxic dose showed consistently very high levels of %Δ (averaging 187.1), in those exposed to 25 μg/mL CeO_2NPs the ROS values increased slightly, reaching a maximum at 14 days (more than double compared to the control). Subsequently, the ROS levels gradually decreased for both doses, without reaching the basal condition at 35 days (%Δ = 52.7 and 83.3, respectively). For both doses, however, ROS production returned to basal levels in the cell progeny grown for 7 days in the absence of nanoceria.

To verify whether ROS overproduction was directly attributable to the pro-oxidant capabilities of the xenobiotic or induced by mitochondrial impairment, transmembrane potential (ΔΨm) was measured. Fig. 2B reports the observed values expressed as %Δ that underline the dose dependent decrease of ΔΨm. After acute nanocera exposure, the %Δ were −20.3 and −30.2 after exposure to the low and high CeO_2NP dose, respectively. Initially, a partial adaptation of the cell progeny was observed which, however, was temporary, highlighting a significant mitochondrial impairment after three weeks ($p < 0.01$ for both doses). Up to the 35th day of observation, basal conditions were not restored and, surprisingly, even in the absence of exposure to the xenobiotic for seven days, a non-negligible mitochondrial dysfunction was still observed.

To assess DNA damage, the alkaline version of the Comet assay was performed. Fig. 2C reports the results expressed as %Δ of TM. After adjusting for cell mortality, the values highlighted both the significant dose-effect correlation ($p = 0.03$) and the distinct pattern between the two nanoceria doses. While the DNA damage induced by the sub-toxic dose was very reduced and no longer appreciable by the 14th day, the one caused by the toxic dose significantly increased starting from the 14th day and remained consistently elevated throughout the observation period. In the post-exposure subculture, DNA damage, although not massive, was still significant ($p < 0.01$).

The cytotoxicity, triggered by sub-chronic exposure to nanoceria, was evaluated measuring spectrofluorimetrically the cells detached from monolayers and PI loaded. Fig. 2D reports the results after acute and sub-chronic exposure. As expected, after acute exposure the % of detached cells was 1.18 and 1.45-fold higher than control cells at the two doses, confirming the MTT results. After sub-chronic exposure, nanoceria caused an average of 20 % more cell mortality at the sub-toxic dose while, at the higher dose, a steady rise in cellular mortality was observed until the second week (% of death cells about 4 times higher; $p = 0.011$). Prolonging the exposure, the values slightly decreased, but remained significantly high throughout the examined period, highlighting the irreversible cell damage. This was confirmed by the values observed in the cell progeny grown for a week in the absence of the toxic. Unlike the progeny of cells exposed to the sub-toxic dose, where there was a complete return to baseline conditions, cell mortality was still 56 % higher in the progeny of cells exposed to the highest dose.

During the acute and sub-chronic exposure, the weekly cell replication index (WCRI) was also evaluated to confirm the cytotoxic effects of the two CeO_2NP doses assayed. To this aim, for each subculture the same number of cells was incubated and, in comparison to control cells, the nanoceria exposure at sub-toxic dose caused a moderate decrease of the WCRI value (5.58 ± 1.05 vs. 6.01 ± 0.85) recording on average 7 % drop. Instead, at the toxic dose of CeO_2NPs, the WCRI was only 4.99 ± 1.20, highlighting a decrease equal to 17 %.

3.4. ^{1}H NMR metabolic profile of cell extracts

A representative ^{1}H NMR spectrum of A549 cell extracts from the control group is shown in Fig. 3. Several polar metabolites were identified, including amino acids such as glycine, glutamine, cysteine, proline, valine, leucine, and isoleucine; osmolytes and methyl donors such as betaine; energy-related metabolites such as glucose, lactate, and succinate; intermediates of the tricarboxylic acid cycle (TCA), including malonate and isocitrate; and signaling-related compounds including choline, acetylcholine, and serotonin.

3.4.1. Pathway enrichment and biological networks

A global pathway enrichment analysis was conducted by integrating all significantly altered metabolites ($p < 0.05$) across doses (25 and 60 μg/mL CeO_2NP) and experimental conditions, including acute exposure (24 h), sub-chronic exposure (examining at 35 days the 5th cell progeny), and recovery in cell progeny grown in CeO_2NP absence. This integrative approach allowed the identification of the metabolic pathways most consistently affected by CeO_2NP exposure over time and across doses (Fig. 4 A). Specifically, the pathway enrichment analysis (SMPDB, 99 sets) demonstrated that nanoceria exposure induces a coordinated reprogramming of A549 cell metabolism. The most significantly CeO_2 NP-affected pathways involved the TCA cycle, pyruvate metabolism, and glycolysis/gluconeogenesis, consistent with ^{1}H NMR evidence of altered glucose, lactate, succinate, and isocitrate, pointing to mitochondrial dysfunction and impaired oxidative metabolism. Perturbations in glutathione, glycine/serine/threonine, and arginine/proline metabolism reflected redox imbalance and amino acid depletion, while enrichment of the Warburg effect confirmed a shift toward aerobic glycolysis. Additional alterations in betaine metabolism, phosphatidylethanolamine biosynthesis, and nicotinate/nicotinamide metabolism indicated changes in membrane remodeling, osmoprotection, and redox cofactor balance. The enrichment dot plot (Fig. 4 A) ranked these pathways by significance, highlighting energy metabolism and antioxidant defences as the most impacted clusters. Network analysis (Fig. 4B) reinforced this view, identifying the TCA cycle, pyruvate metabolism, glutathione metabolism, and glycine/serine/threonine metabolism as central hubs connecting bioenergetics, redox regulation, and amino acid turnover. Together, these analyses demonstrate that CeO_2NP exposure remodels the metabolic landscape through integrated disruption of mitochondrial, redox, and amino acid pathways, reflecting a balance between transient adaptive responses and persistent dysfunction under prolonged or higher dose conditions.

3.4.2. Multivariate analysis of metabolomic profiles

A Principal Component Analysis (PCA) was performed to evaluate global variance structure and the overall similarity of metabolic profiles across exposure conditions. The PCA score plot (Fig. 5 A) revealed a clear dose- and time-dependent separation among the experimental groups, in agreement with the univariate findings. After 24 h, cells exposed to 60 μg/mL diverged markedly from both control and 25 μg/mL samples. Sub-chronic exposure further amplified these differences as, at the toxic dose, the subculture examined at 35 days clustered in a distinct region of the PCA space. In contrast at 25 μg/mL, the one examined at 35 days remained closer to controls. Recovery dynamics were also captured by the PCA. Progeny previously exposed to 25 μg/mL and subsequently grown for 7 days in nanoparticle-free medium clustered near control samples. Conversely, progeny recovered after sub-chronic exposure to 60 μg/mL remained clearly separated from both control and 25 μg/mL groups. The PCA loading vectors (Fig. 5B) highlighted metabolites like lactate, betaine, cysteine, serotonin, and acetylcholine, together with glutathione and glutamine, as major contributors to the separation among groups, mirroring the patterns

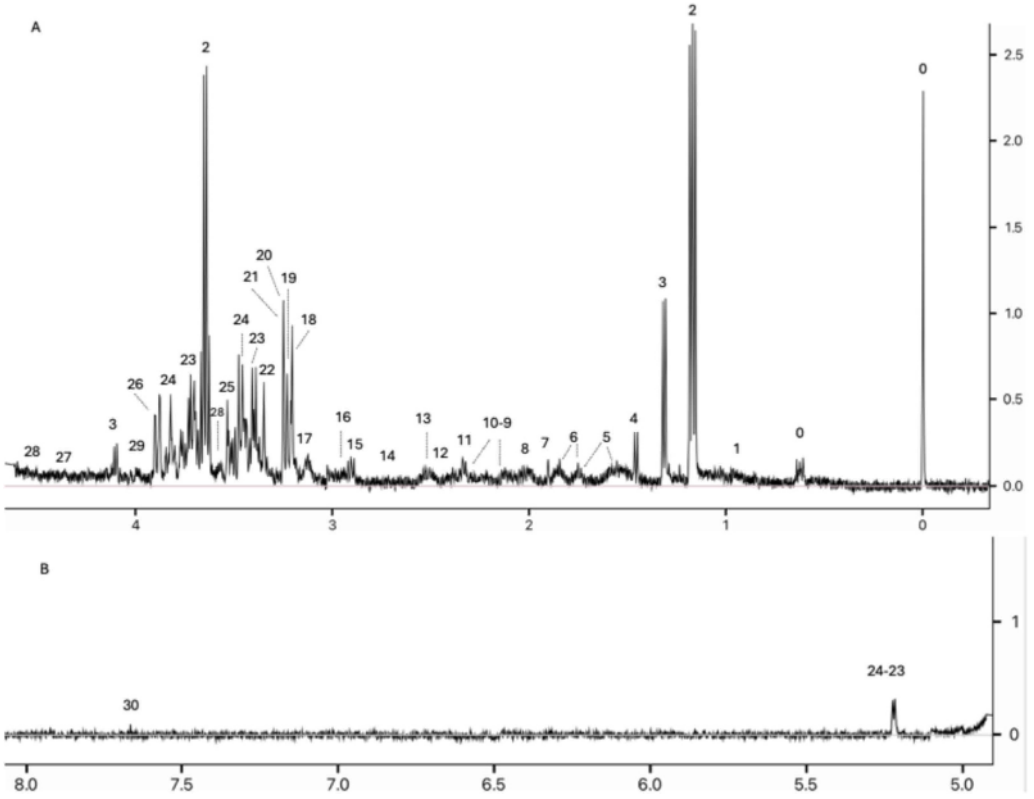

Fig. 3. A representative 1-D 500 MHz ^{1}H NMR spectrum of human alveolar A549 control cells, from which the residual water resonances (4.5–5.0 ppm) were removed, and with (A) showing the aliphatic region, and (B) an expansion of the aromatic region. Keys: (0) DSS, (1) branched chain amino acids (BCAA: isoleucine, leucine and valine), (2) ethanol, (3) lactate, (4) alanine, (5) arginine, (6) lysine, (7) acetate, (8) proline, (9) glutamate, (10) glutamine (11) succinate, (12) malate, (13) isocitrate, (14) aspartate, (15) N,N-Dimethylglycine, (16) glutathione (17) malonate, (18) choline, (19) acetylcholine, (20) betaine, (21) trimethylamine N-oxide (TMAO), (22) taurine, (23) glucose, (24) maltose, (25) glycine, (26) creatine, (27) ATP/ADP, (28) serotonin, (29) tyrosine, and (30) methylhistidine.

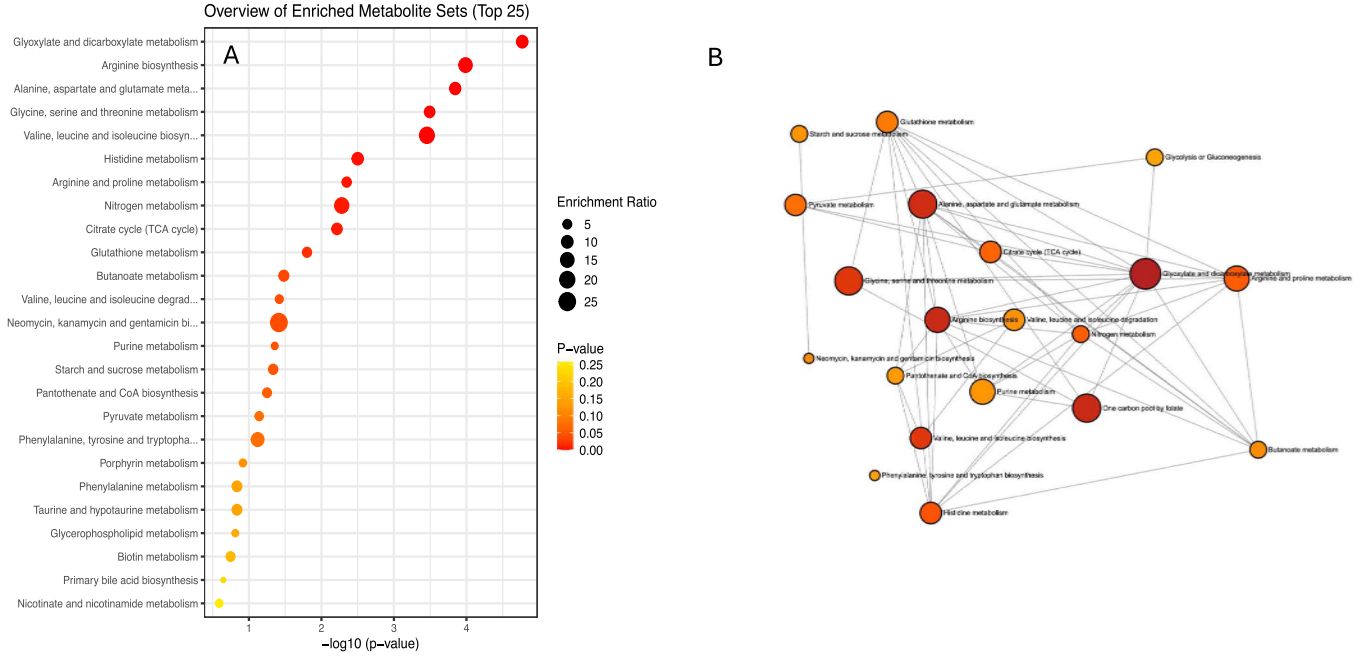

Fig. 4. (A) Global pathway enrichment analysis of human alveolar A549 cells exposed to CeO_2NP ($\leq$ 50 nm) under different exposure conditions: acute (24 h) and sub-chronic exposure (35 days of continuous exposure) at 25 and 60 µg/mL CeO_2NP, and recovery in cell progeny grown in CeO_2NP absence. The analysis (SMPDB, 99 sets; over-representation analysis, hypergeometric test, FDR correction) was based on all significantly altered metabolites ($p < 0.05$) across conditions and identified the most consistently affected pathways related to energy metabolism, redox regulation, and amino acid turnover. (B) Pathway network analysis of enriched pathways (KEGG database; topology-based analysis, $p < 0.05$, FDR correction). Central hubs (TCA, pyruvate, glutathione metabolism) highlight coordinated disruption of mitochondrial, redox, and amino acid pathways.

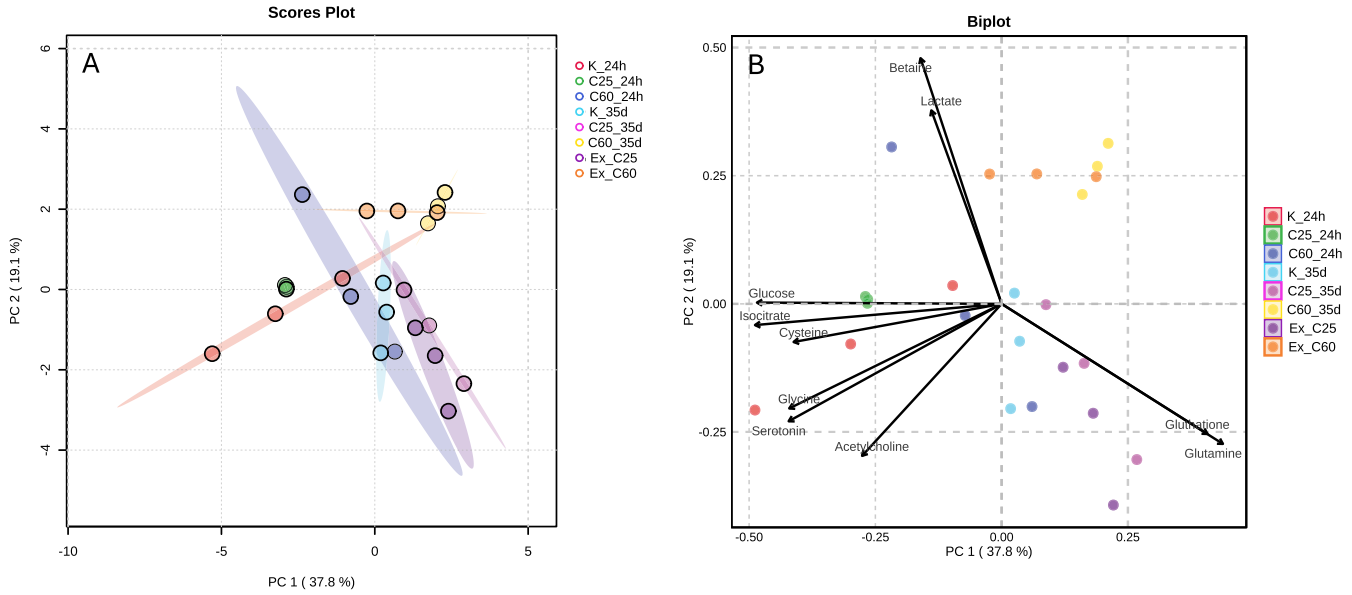

Fig. 5. (A) Principal Component Analysis (PCA) score plot of metabolomic profiles from A549 cells exposed to CeO_2NPs ($\leq$ 50 nm) at 25 and 60 μg/mL under acute (24 h), sub-chronic (35 days), and recovery conditions. Data were log-transformed and Pareto-scaled prior to analysis. (B) PCA biplot showing score distribution and loading vectors of metabolites contributing to the separation of A549 cell groups following CeO_2NP exposure at 25 and 60 μg/mL under acute (24 h), sub-chronic (35 days), and recovery conditions. Metabolomic data were log-transformed and Pareto-scaled. The loading vectors indicate the metabolites contributing most to variance along PC1 and PC2, with lactate, betaine, glutamine, glutathione, glycine, cysteine, serotonin, and acetylcholine acting as major discriminators between groups.

identified through the heatmap and enrichment analyses.

3.4.3. *Cell metabolome changes*

Several metabolic pathways were found to be affected in A549 cells following exposure to nanoceria. In particular, ^{1}H NMR-based metabolomic analysis revealed dose- and time-dependent alterations in key metabolites involved in energy production, redox balance, and membrane turnover (Fig. 6). The fluctuations in metabolite concentrations across samples and experimental conditions were further clarified through a correlation heatmap (Fig. 7), which displayed distinct clustering patterns among control, sub-toxic (25 μg/mL), and toxic (60 μg/mL) groups. The heatmap clearly highlighted coordinated variations in metabolite levels, illustrating the progressive metabolic shift induced by CeO_2NP exposure over time and with increasing concentration.

After 24 h of exposure, metabolite profile changed according to the two tested CeO_2NP doses. At the lower dose (25 μg/mL), a significant increase ($p < 0.05$) compared to control cells was observed in several metabolites, including glucose, lactate, succinate, isocitrate, malonate, glycine, glutamine, glutathione, cysteine, acetylcholine, serotonin, and betaine, except for choline whose levels were similar to those of control cells. Conversely, an opposite trend was recorded in cell samples exposed to the higher CeO_2NP concentration (60 μg/mL), where mostly metabolites showed a decrease in respect to control cells (Fig. 6).

Notably, after 35 days of continuous exposure, the cell progeny exhibited a distinctly impaired metabolic profile, with a reduction in glycine, cysteine, serotonin, acetylcholine, glucose, and succinate levels at both CeO_2NP concentrations in respect to control cells. In parallel, the levels of lactate, malonate, and glutamine were elevated than in control cells. Interestingly, other metabolites showed a biphasic trend, such as glutathione that increased at 25 μg/mL CeO_2NP exposure and dropped at 60 μg/mL, and choline and betaine that exhibited an opposite behaviour. Only isocitrate was found unchanged after 35 days of exposure in all the conditions tested (Fig. 6).

After a 7-day recovery period in the absence of exposure, cell progeny of previously sub-chronically exposed cells for 28 days at the two CeO_2NP doses showed a differential metabolic response. Cell progeny previously treated with 25 μg/mL CeO_2NP and then grown for 7 days in the absence of nanoceria, exhibited mostly of the investigated metabolites with levels superimposable with those registered after 35 days of exposure, except for a significant increase recorded in the level of glutamine in respect also to the control cells. However, in the cells previously exposed to the toxic dose, a partial recovery was observed, with glucose, glycine, isocitrate, and glutathione levels increased, reaching values close to those of control cells, while cysteine, acethylcholine, and serotonin remained steady. Additionally, lactate and betaine showed levels higher than those of the control cells, whereas a significant reduction in choline levels was noticed, resulting in the same concentration recorded in control cells (Fig. 6).

4. Discussion

With the aim to improve our understanding of the potential biological effects of inhaled nanoceria, in this study we used an *in vitro* model resembling both acute and sub-chronic exposure of the human respiratory tract. Since all persistent environmental pollutants are responsible for prolonged exposure over time, we consider our approach particularly useful.

The analysis of CeO_2NP in a biological environment emphasized its strong bioavailability, despite the formation of nano/microaggregates. The absence of surface charges in a biological environment is attributable to both pH and osmotic pressure. The observations of Mu et al. [37] support this, indicating that a pH of 7.4 in water yields a ζ-potential of + 10–15 mV. The nanoparticles' low surface charge is likely neutralized in a biological environment by the salts in the PBS and cell medium, making both solutions isotonic.

The strong nanoceria hydrophobicity, resulting from the absence of surface charges, enhanced its capacity to interact with biological membranes, as shown by the fast uptake, previously demonstrated on the same cell line for other hydrophobic xenobiotic particles, such as carbon nanotubes and micro- and nanoplastics [15,38,39].

The quick dose-dependent absorption of CeO_2NPs by alveolar epithelial cells, achieved high values after just 2 h, which increased minimally with prolonged exposure, and only for the subtoxic dose. Instead, the damages to endocytic compartment observed at toxic dose,

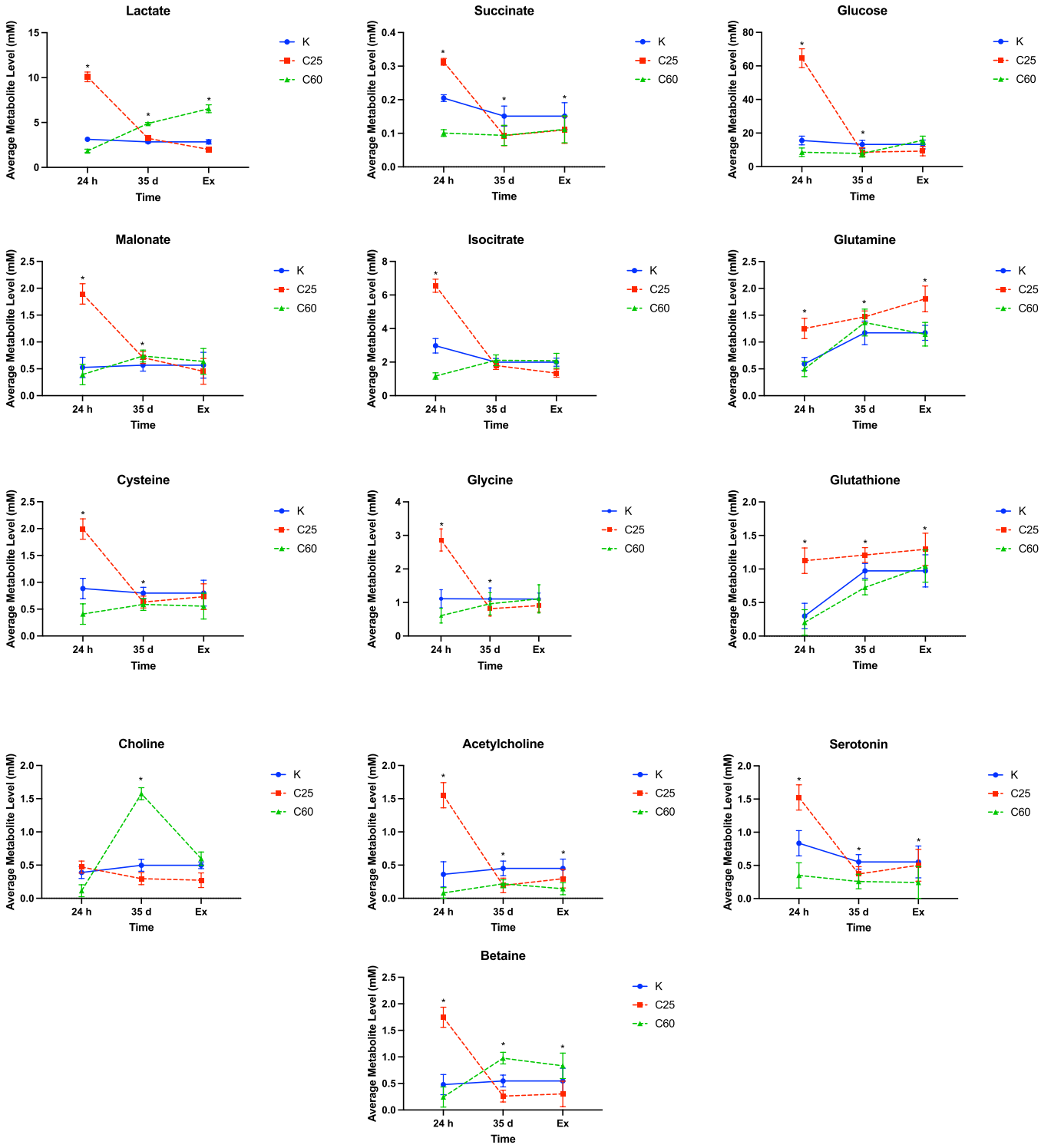

Fig. 6. ^{1}H NMR measurements (mM, mean ± SD) of key metabolites involved in energy production, redox balance, and membrane turnover in human alveolar A549 cells exposed to CeO_2NPs (≤50 nm). Data show dose- and time-dependent metabolic alterations. Asterisks indicate significant differences compared to the control (Dunnett's test; * $p < 0.05$).

and shown by the decrease in green emission, would seem to highlight how even mechanical injury, causing acidification of the cytosol, can contribute to the increased cell mortality [15].

It is still crucial to emphasize that the analyses of endocytic compartment may underestimate uptake since it excludes the internalization of nanoparticles by passive diffusion across the phospholipid bilayer, resulting in their presence both individually and in aggregates inside the cytosol. Given the high hydrophobicity of CeO_2NPs in a biological context, this mechanism of 'internalization' should not be disregarded [39].

Interestingly, the combination of conventional toxicological assays and metabolomics-based approaches provided a comprehensive picture of the impact of CeO_2NPs on human alveolar cells. In general, the nanoceria particles tested induced dose- and time-dependent effects on cellular functionality, highlighted by standard toxicity tests, and confirmed by the fluctuations in the levels of specific metabolites. In

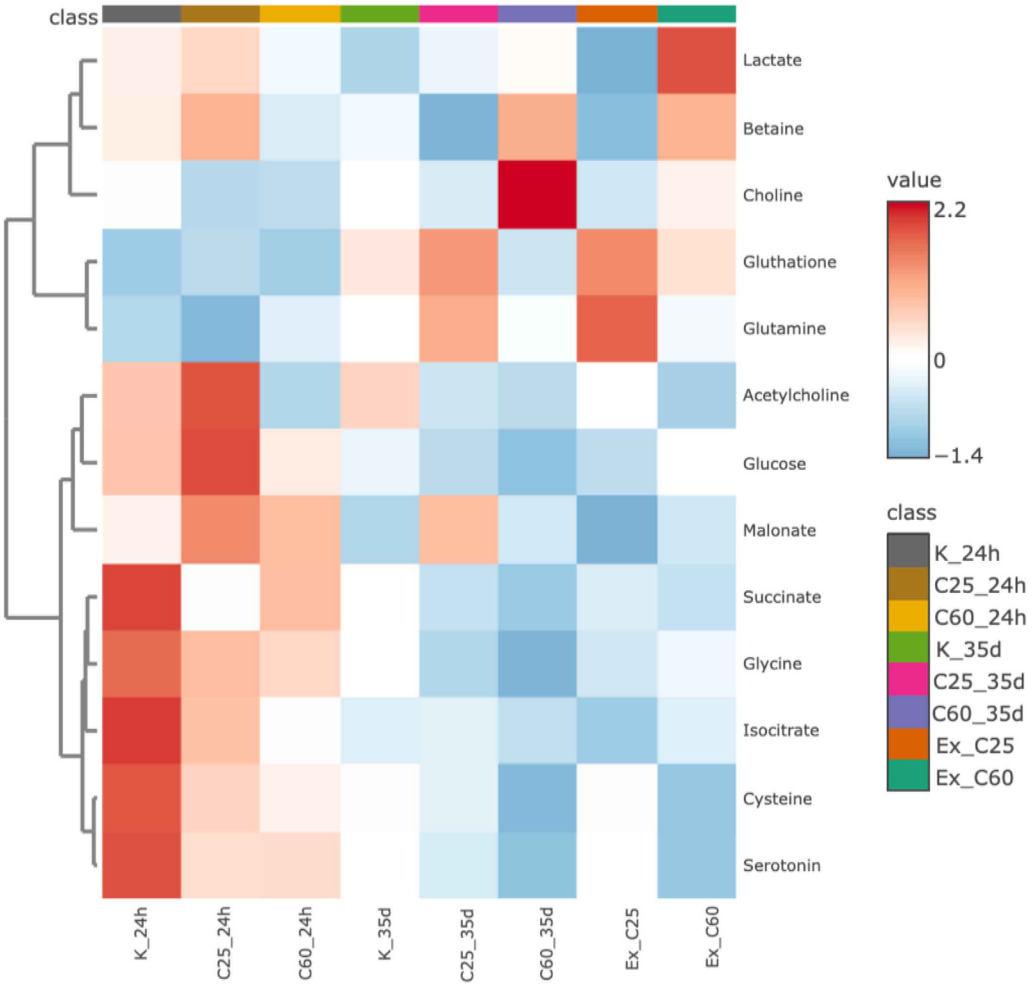

Fig. 7. Correlation heatmap of metabolite concentrations in human alveolar A549 cells exposed to CeO_2NPs (≤50 nm) at 25 and 60 μg/mL for 24 h and 35 days, and after 7 days of recovery. The heatmap illustrates dose- and time-dependent clustering patterns among control, sub-toxic, and toxic groups, highlighting coordinated variations in metabolites involved in energy production, redox balance, and membrane turnover. Each row represents a specific metabolite, while each column corresponds to one of the experimental conditions. Colour intensity indicates the direction and magnitude of change, with red shades representing increased metabolite levels, whereas blue shades indicating decreased levels compared to control.

particular, the moderate cytotoxicity and slight increase in ROS and ROS-induced effects observed through toxicological assays after 24 h at the subtoxic dose was confirmed by the metabolic profile suggesting an initial adaptive response. The generalized metabolic activation is likely aimed at meeting energy demands, counteracting oxidative stress, and promoting repair of cellular structures. Several upregulated metabolites, such as glucose, lactate, succinate, glutamate, glutamine, glycine, and glutathione, play key roles in sustaining the metabolic plasticity of A549 cells, which heavily rely on glycolysis and glutaminolysis to support proliferation and survival [40,41]. In particular, the accumulation of lactate reflects the Warburg effect, whereby glucose is preferentially converted to lactate even under normoxic conditions [42], a hallmark of A549 and other lung cell lines that supports rapid ATP production and NAD^+ regeneration [43,44]. Conversely, the depletion of metabolite levels at the toxic dose (60 μg/mL CeO_2NPs) confirmed the most severe early mitochondrial dysfunction, consistent with initial signs of bioenergetic failure as shown by the reduced metabolic capacity. The suppression of key metabolites such as glucose, succinate, choline, glutathione, and amino acids suggests an impaired ability to sustain oxidative metabolism and energy production (*i.e.* a dyshomeostasis status). Such metabolic shutdowns, confirmed by the ΔΨm values and the higher level of cell mortality, have previously been associated with mitochondrial depolarization and apoptotic induction in lung cell models [38,45-47].

Toxicological tests over time validated the significant dose-effect correlation and the enhanced capacity of cell progeny exposed to the sub-toxic dose to counteract the overproduction of ROS and the ensuing ROS-induced cytotoxic effects, as highlighted by the full recovery of DNA damage and the partial recovery of mitochondrial dysfunction, despite a transient increase in values in the first phase of sub-chronic exposure. Conversely, as shown by the highest treated/control mortality ratio, the effects induced by the toxic dose was irreversible for a consistent portion of the exposed cell progeny, suggesting tissue damage in exposed individuals following the exhaustion of regenerative capacity. This ultimately results in the gradual substitution of functioning epithelium with fibrotic tissue, leading to significant respiratory failure. Several airborne xenobiotics have been increasingly implicated in impairing lung tissue function, through pro-fibrotic myofibroblast expansion. This irreversibly narrows the airways causing pulmonary fibrosis and chronic obstructive pulmonary disease (COPD) [48].

As expected, a progressively compromised metabolic profile was observed after sub-chronic exposure, with marked reductions at 35 days in glycine, cysteine, serotonin, and acetylcholine at both concentrations. Glycine and cysteine are central precursors for glutathione biosynthesis, and their depletion, not coupled with increased glutathione production, as observed at the toxic dose, reflects a profound redox imbalance and exhaustion of antioxidant reserves [33,49–51]. The biphasic trend of glutathione, with increased levels at 25 μg/mL but significant depletion

at 60 μg/mL CeO_2NPs in respect to control cells, highlights as the lower dose triggers an antioxidant response able to counteract, although not completely, the biological effects of nanoceria.

The decrease in serotonin and acetylcholine levels may indicate disrupted signaling and biosynthetic stress, potentially contributing to impaired cell viability and communication. The increased choline level at the toxic dose of CeO_2NPs was indicative of phospholipid degradation and membrane damage processes, as confirmed by the rise of dead cells and previously documented by Pan et al. [43] in the same cell line. These alterations were accompanied by significant decreases in glucose and succinate, along with marked increases in lactate and malonate at the toxic dose, and glutamine at both doses, suggesting a metabolic shift toward anaerobic glycolysis and disruption of the tricarboxylic acid (TCA) cycle. The significant accumulation of glutamine at sub-toxic dose suggest compensatory activation of glutaminolysis, likely as a survival mechanism in response to mitochondrial dysfunction, as previously demonstrated in metabolomic studies of A549 cells exposed to fumed silica nanoparticles [52]. Beyond their role in cellular energy generation, mitochondria and the TCA cycle provide critical molecular hubs for a variety of cellular functions, including biosynthesis, signaling, apoptosis, and immune responses [53–57]. This explains as the metabolic profile is related to the mitochondrial collapse, more marked at the higher dose and previously observed in the same cell line exposed to tetrabromobisphenol A (TBBPA) [58]. Overall, the metabolomic alterations following sub-chronic exposure were in agreement with the dose-related levels of cytotoxicity, oxidative stress, mitochondrial impairment, and decreased replication index. Disruption of metabolic and redox homeostasis was strongly linked to the observed inhibition of cell regeneration and proliferation [59], and consistent with findings from other *in vitro* study investigating the cytotoxic responses of lung cells to metal-based compounds [60].

Post-exposure experiments further confirmed the differential responses at the two CeO_2NP doses. At 25 μg/mL, toxicological results and metabolite levels in general, underlined a good recovery of baseline values, showing cellular adaptation to this nanoceria dose. Conversely, at 60 μg/mL CeO_2 NPs, the recovery was very limited. Despite the partial reactivation of the antioxidant system, shown by the increased levels of glycine and glutathione and confirmed by ROS values, approaching control values, cysteine and serotonin remained depleted. This suggests that full redox balance was not restored. The exposure at the toxic dose of CeO_2NPs did not allow to restore DNA integrity and mitochondrial functionality in cell progeny grown in absence of nanoceria while, at the metabolic level, reduction in choline and betaine levels suggest ongoing membrane remodelling processes, which may reflect structural recovery attempts. These post-exposure metabolic shifts underscore the impact of sub-chronic nanoceria exposure on cellular homeostasis and may serve as potential metabolic signatures of irreversible damage versus effective adaptation.

In line with these findings, pathway enrichment and network analyses provided a systems-level confirmation, consistently highlighting mitochondrial energy metabolism, redox regulation, and amino acid turnover as central hubs reprogrammed by nanoceria exposure.

5. Conclusions

These findings confirm that CeO_2NP exposure significantly alters cellular metabolism, causing several biological effects strongly related with both dose and exposure duration. Specifically, the combination of conventional toxicological tests and metabolomic analysis allowed us to highlight as fluctuations in specific metabolites may be interpreted either as transient adaptive responses or, conversely, as indicators of persistent damage, particularly under conditions of prolonged high-dose exposure. Despite a variable capacity for cellular homeostasis was evident, the results shed light on the potential risks of exposure to these ubiquitous xenobiotics to human health.

However, it is likely that the doses of nanoceria tested do not allow us to infer the results obtained for the general population, as pollution levels of this emerging xenobiotic are poorly known, and even less predictable are the exposures in the near future. Considering the peculiarities of the nanoceria, it is nonetheless plausible to expect its more widespread and higher inhalation exposure, both occupational and for the general population. The pathogenic role of airborne respirable particles (PM 2.5 and 0.1 μm) in both respiratory and systemic diseases is well known, therefore a more comprehensive understanding of the toxicological potential of nanoceria is quite crucial, making our results a useful starting point.

Environmental Implication

In a society focused on sustainability, green technologies expand usage of Rare Earth Elements. Cerium dioxide nanoparticles (CeO_2NPs) possess redox/catalytic activity but raise inhalation concerns. This study unveils the CeO_2NPs effects in alveolar A549 cells exposed to 25 and 60 μg/mL as 37 % and 89 % of IC50, respectively, for 24 h (acute exposure) and 35 days (sub-chronic exposure), besides evaluating recovery in progeny of exposed cells grown in CeO_2NPs absence. Nanoceria triggered concentration- and time-dependent cytotoxic, oxidative, mitochondrial, genotoxic, and metabolic alterations in A549 cells. Due to its dual antioxidant/pro-oxidant role, nanoceria is an emerging inhalable pollutant for human health.

CRediT authorship contribution statement

Angela Di Pietro: Writing – review & editing, Validation, Supervision, Resources, Methodology, Conceptualization. **Alessio Facciolà:** Software, Methodology, Formal analysis, Data curation. **Antonio Laganà:** Writing – original draft, Software, Formal analysis, Data curation. **Barbara Billè:** Writing – original draft, Visualization, Software, Formal analysis, Data curation, Conceptualization. **Daniela Iannazzo:** Formal analysis. **Consuelo Celesti:** Formal analysis. **Mariachiara Galati:** Software, Methodology, Formal analysis. **Maria Maisano:** Writing – review & editing, Validation, Resources, Methodology. **Tiziana Cappello:** Writing – review & editing, Validation, Supervision, Software, Methodology, Data curation, Conceptualization. **Giuseppa Visalli:** Writing – review & editing, Software, Methodology, Data curation, Conceptualization.

Ethic approval

No approval of research ethic committees was required to accomplish the goals of this study since the experimental work was conducted using an *in vitro* model resembling pulmonary cells.

Declaration of Competing Interest

The authors declare that they have no known competing financial interests or personal relationships that could have appeared to influence the work reported in this paper.

Appendix A. Supporting information

Supplementary data associated with this article can be found in the online version at doi:10.1016/j.jhazmat.2026.141239.

Data availability

Data will be made available on request.

References

[1] Depraiter, L., Goutte, S., 2023. The role and challenges of rare earths in the energy transition. Resour Pol 86, 104137.

[2] Balaram, A., 2019. Rare earth elements: a review of applications, occurrence, exploration, analysis, recycling, and environmental impact. Geosci Front 10 (4), 1285–1303.

[3] Falvo, S., Grillo, G., Venditti, M., Chieffi Baccari, G., Di Fiore, M.M., Cappello, T., et al., 2025. Gadolinium impairs male stereoidogenesis: *in vivo* and *in vitro* evidence. Toxicol 518, 154261.

[4] Falvo, S., Grillo, G., Venditti, M., Chieffi Baccari, G., Di Fiore, M.M., Cappello, T., et al., 2026. Toxic effects of gadolinium on spermatogenesis are associated with inflammation, oxidative stress, apoptosis and autophagy. Toxicology 519, 154335.

[5] Gwenzi, W.L., Mangori, C., Danha, N., Chaukura, N., Dunjana, E., Sanganyado, 2018. Sources, behaviour, and environmental and human health risks of high-technology rare earth elements as emerging contaminants. Sci Total Environ 636, 299–313.

[6] Piarulli, S., Hansen, B.H., Ciesielski, T., Zocher, A., Malzahn, A., Olsvik, P.A., et al., 2021. Sources, distribution and effects of rare earth elements in the marine environment: current knowledge and research gaps. Environ Pollut 291, 118230.

[7] Xue, Y., Balmuri, S.R., Patel, A., Sant, V., Sant, S., 2018. Synthesis, physico-chemical characterization, and antioxidant effect of PEGylated cerium oxide nanoparticles. Drug Deliv Transl Res 8, 357–367.

[8] Reed, K., Cormack, A., Kulkarni, A., Mayton, M., Sayle, D., Klaessig, F., et al., 2014. Exploring the properties and applications of nanoceria: is there still plenty of room at the bottom? Environ Sci Nano 1, 390–405.

[9] Trovato, M.C., Andronico, D., Sciacchitano, S., Ruggeri, R.M., Picerno, I., Di Pietro, A., et al., 2018. Nanostructures: between natural environment and medical practice. Rev Environ Health 33 (3), 295–307.

[10] Saifi, M.A., Seal, S., Godugu, C., 2021. Nanoceria, the versatile nanoparticles: promising biomedical applications. J Control Release 338, 164–189.

[11] IBU-tec D.E.U., Cerium Oxide. IBUpart® CeO2. ⟨https://www.ibu-tec.com⟩ ⟩ products ⟩ cerium-oxide-ceo2 (Accessed 20 January 2025).

[12] Heckert, E.G., Seal, S., Self, W.T., 2008. Fenton-like reaction catalyzed by the rare Earth inner transition metal cerium. Environ Sci Technol 42 (13), 5014–5019.

[13] Eliso, M.C., Billè, B., Cappello, T., Maisano, M., 2024. Polystyrene micro-and nanoplastics (PS MNPs): a review of recent advances in the use of-omics in PS MNP toxicity studies on aquatic organisms. Fishes 9 (3), 98.

[14] Laganà, A., Billè, B., Visalli, G., Facciolà, A., Cappello, T., Maisano, M., et al., 2025. Toxicological assays and metabolomic profiling to evaluate the effects of virgin and aged micro- and nano- polystyrene plastics in SH-SY5Y human neuroblastoma cells. Sci Total Environ 975, 179262.

[15] Laganà, A., Visalli, G., Facciolà, A., Celesti, C., Iannazzo, D., Di Pietro, A., 2023. Uptake of breathable nano- and micro-sized polystyrene particles: comparison of virgin and oxidised nPS/mPS in human alveolar cells. Toxics 11, 686.

[16] Remigante, A., Spinelli, S., Gambardella, L., Bozzuto, G., Vona, R., Caruso, D., et al., 2024. Internalization of nano- and micro-plastics in human erythrocytes leads to oxidative stress and estrogen receptor-mediated cellular responses. Free Radic Biol Med 223, 1–17.

[17] Sangomla, S., Saifi, M.A., Khurana, A., Godugu, C., 2018. Nanoceria ameliorates doxorubicin induced cardiotoxicity: possible mitigation via reduction of oxidative stress and inflammation. J Trace Elem Med Biol 47, 53–62.

[18] Shokrzadeh, M., Abdi, H., Asadollah-Pour, A., Shaki, F., 2016. Nanoceria attenuated high glucose-induced oxidative damage in HepG2 cells. Cell J Spring 18 (1), 97–102.

[19] Khurana, A., Saifi, M.A., Godugu, C., 2023. Nanoceria ameliorates fibrosis, inflammation, and cellular stress in experimental chronic pancreatitis. ACS Biomater Sci Eng 9 (2), 1030–1042.

[20] Yokel, R.A., Hussain, S., Garantziotis, S., Demokritou, P., Castranova, V., Cassee, F. R., 2014. The Yin: an adverse health perspective of nanoceria: uptake, distribution, accumulation, and mechanisms of its toxicity. Environ Sci Nano 1 (5), 406–428.

[21] Mousavi-Kouhi, S.M., Beyk-Khormizi, A., Amiri, M.S., Mashreghi, M., Hashemzadeh, A., Mohammadzadeh, V., et al., 2023. Plant gel-mediated synthesis of gold-coated nanoceria using *Ferula gummosa*: characterization and estimation of its cellular toxicity toward breast cancer cell lines. J Funct Biomater 14 (7), 332.

[22] Hirst, S.M., Karakoti, A., Singh, S., Self, W., Tyler, R., Seal, S., et al., 2013. Bio-distribution and in vivo antioxidant effects of cerium oxide nanoparticles in mice. Environ Toxicol (2), 107–118.

[23] Fraga-Corral, M., Carpena, M., Garcia-Oliveira, P., Pereira, A.G., Prieto, M.A., Simal-Gandara, J., 2022. Analytical metabolomics and applications in health, environmental and food science. Crit Rev Anal Chem 52 (4), 712–734.

[24] Afsa, S., Maisano, M., Germanà, A., Cappello, T., 2025. Polystyrene microplastics (PS-MPs): a review on metabolic disruptions and potential obesogenic implications using -omics approaches based evidences on zebrafish model. Environ Res 284, 122236.

[25] Eliso, M.C., Billè, B., De Marco, G., Pulvirenti, E., Dal Bello, F., Rapisarda, P., et al., 2025. Embryotoxicity of polystyrene microplastics, alone and conjugated with bisphenol A, in the black sea urchin *Arbacia lixula*: a multi-biomarker approach. J Hazard Mater 499, 140139.

[26] Cappello, T., 2020. NMR-based metabolomics of aquatic organisms. In: eMagRes, section of Environmental & Ecological NMR, 9. John Wiley & Sons, Ltd, pp. 81–100.

[27] Iannazzo, D., Pistone, A., Celesti, C., Triolo, C., Patané, S., Giofré, S.V., et al., 2019. A Smart nanovector for cancer targeted drug delivery based on graphene quantum dots. Nanomaterials 9 (2), 282.

[28] Di Pietro, A., Visalli, G., Baluce, B., Micale, R.T., La Maestra, S., Spataro, P., et al., 2011. Multigenerational mitochondrial alterations in pneumocytes exposed to oil fly ash metals. Int J Hyg Environ Health 214 (2), 138–144.

[29] Visalli, G., Laganà, A., Facciolà, A., Iaconis, A., Curcio, J., Pollino, S., et al., 2023. Enhancement of biological effects of oxidised nano- and microplastics in human professional phagocytes. Environ Toxicol Pharm 99, 104086.

[30] Missawi, O., Venditti, M., Cappello, T., Zitouni, N., De Marco, G., Boughattas, I., et al., 2022. Autophagic event and metabolomic disorders unveil cellular toxicity of environmental microplastics on marine polychaete *Hediste diversicolor*. Environ Pollut 302, 119106.

[31] Cappello, T., De Marco, G., Oliveri Conti, G., Giannetto, A., Ferrante, M., Mauceri, A., et al., 2021. Time-dependent metabolic disorders induced by short-term exposure to polystyrene microplastics in the Mediterranean mussel *Mytilus galloprovincialis*. Ecotoxicol Environ Saf 209, 111780.

[32] Caricato, R., Giordano, M.E., Schettino, T., Maisano, M., Mauceri, A., Giannetto, A., et al., 2019. Carbonic anhydrase integrated into a multimarker approach for the detection of the stress status induced by pollution exposure in *Mytilus galloprovincialis*: a field case study. Sci Total Environ 690, 140–150.

[33] Zitouni, N., Cappello, T., Missawi, O., Boughattas, I., De Marco, G., Belbekhouche, S., et al., 2022. Metabolomic disorders unveil hepatotoxicity of environmental microplastics in wild fish *Serranus scriba* (Linnaeus 1758). Sci Total Environ 838, 155872.

[34] De Marco, G., Brandão, F., Pereira, P., Pacheco, M., Cappello, T., 2022. Organ-specific metabolome deciphering cell pathways to cope with mercury in wild fish (golden grey mullet *Chelon auratus*). Animals 12, 79.

[35] De Marco, G., Cristaldi, A., Eliso, M.C., Oliveri Conti, G., Galati, M., Billè, B., et al., 2025. Cellular pathway disturbances elicited by realistic dexamethasone concentrations in gills of mussel *Mytilus galloprovincialis* as assessed by a multi-biomarker approach. Environ Toxicol Pharm 113, 104598.

[36] Chong, J., Wishart, D.S., Xia, J., 2019. Using MetaboAnalyst 4.0 for comprehensive and integrative metabolomics data analysis. Curr Protoc Bioinf 68 (1), e86.

[37] Mu, L., Ghorbani, M., Baveye, F.C., Darnault, C.J.G., 2024. Colloid systems and interfaces stability of cerium oxide nanoparticles in aqueous environments: effects of pH, ionic composition, and Suwanee river humic and fulvic acids. J Nanomater 30, 2970861.

[38] Visalli, G., Baluce, B., Bertuccio, M., Picerno, I., Di Pietro, A., 2015. Mitochondrial-mediated apoptosis pathway in alveolar epithelial cells exposed to the metals in combustion-generated particulate matter. J Toxicol Environ Health A 78 (11), 697–709.

[39] Visalli, G., Facciolà, A., Iannazzo, D., Piperno, A., Pistone, A., Di Pietro, A., 2017. The role of the iron catalyst in the toxicity of multi-walled carbon nanotubes (MWCNTs). J Trace Elem Med Biol 43, 153–160.

[40] Duarte, I.F., Ladeirinha, A.F., Lamego, I., Gil, A.M., Carvalho, L., Carreira, I.M., et al., 2013. Potential markers of cisplatin treatment response unveiled by NMR metabolomics of human lung cells. Mol Pharm 10 (11), 4242–4251.

[41] Panieri, E., Santoro, M.M., 2016. ROS homeostasis and metabolism: a dangerous liason in cancer cells. Cell Death Dis 7 (6) e2253-e2253.

[42] Warburg, O., Wind, F., Negelein, E., 1927. The metabolism of tumors in the body. J Gen Physiol 8 (6), 519.

[43] Pan, T., Han, D., Xu, Y., Peng, W., Bai, L., Zhou, X., et al., 2021. LC–MS based metabolomics study of the effects of EGCG on A549 cells. Front Pharm 12, 732716.

[44] Tavares, L.C., Amorim, R., Teixeira, J., Oliveira, P.J., Carvalho, R.A., 2025. Metabolic profile of human non-small cell lung cancer cells through combined 13C and ^{2}H NMR. BBA Mol Basis Dis, 167949.

[45] Visalli, G., Facciolà, A., Currò, M., Laganà, P., La Fauci, V., Iannazzo, D., et al., 2019. Mitochondrial impairment Induced by sub-chronic exposure to multi-walled carbon nanotubes. Int J Environ Res Public Health 16 (5), 792.

[46] Rainaldi, G., Romano, R., Indovina, P., Ferrante, A., Motta, A., Indovina, P.L., Santini, M.T., 2008. Metabolomics using 1H-NMR of apoptosis and necrosis in HL60 leukemia cells: Differences between the two types of cell death and independence from the stimulus of apoptosis used. Radiat. Res. 169, 170–180. https://doi.org/10.1667/rr0958.1.

[47] Halama, A., Riesen, N., Möller, G., Hrabë de Angelis, M., Adamski, J., 2013. Identification of biomarkers for apoptosis in cancer cell lines using metabolomics: tools for individualized medicine. J. Intern. Med. 274, 425–439. https://doi.org/10.1111/joim.12117.

[48] Wu, X., Lin, L., Yan, H., Zheng, F., Ding, Y., Yao, H., 2025. Exposure to environmental xenobiotics and lung tissue function: a comprehensive review on biological mechanisms and pathways. Ecotoxicol Environ Saf 308, 119438.

[49] Galadari, S., Rahman, A., Pallichankandy, S., Thayyullathil, F., 2017. Reactive oxygen species and cancer paradox: to promote or to suppress? Free Radic Biol Med 104, 144–164.

[50] Lv, H., Zhen, C., Liu, J., Yang, P., Hu, L., Shang, P., 2019. Unraveling the potential role of glutathione in multiple forms of cell death in cancer therapy. Oxid Med Cell Longev 1, 3150145.

[51] Moloney, J.N., Cotter, T.G., 2018. ROS signalling in the biology of cancer. In: In Seminars in Cell & Developmental Biology, 80. Academic Press, pp. 50–64.

[52] Irfan, A., Cauchi, M., Edmands, W., Gooderham, N.J., Njuguna, J., Zhu, H., 2014. Assessment of temporal dose-toxicity relationship of fumed silica nanoparticle in human lung A549 cells by conventional cytotoxicity and ^{1}H NMR-based extracellular metabonomic assays. Toxicol Sci 138 (2), 354–364.

[53] Fang, T., Wang, M., Xiao, H., Wei, X., 2019. Mitochondrial dysfunction and chronic lung disease. Cell Biol Toxicol 35, 493–502.

[54] Miliotis, S., Nicolalde, B., Ortega, M., Yepez, J., Caicedo, A., 2019. Forms of extracellular mitochondria and their impact in health. Mitochondrion 48, 16–30.

[55] Najahi, H., Alessio, N., Venditti, M., Lettiero, I., Aprile, D., Oliveri Conti, G., et al., 2025. Impact of environmental microplastic exposure on HepG2 cells: unraveling proliferation, mitochondrial dynamics and autophagy activation. Part Fibre Toxicol 22, 17.

[56] Osellame, L.D., Blacker, T.S., Duchen, M.R., 2012. Cellular and molecular mechanisms of mitochondrial function. Best Pract Res Clin Endocrinol Metab 26, 711–723.
[57] Xia, M., Zhang, Y., Jin, K., Lu, Z., Zeng, Z., Xiong, W., 2019. Communication between mitochondria and other organelles: a brand-new perspective on mitochondria in cancer. Cell Biosci 9, 27.
[58] He, H., Pan, T., Shi, X., Yang, S., Jasbi, P., Jin, Y., et al., 2023. An integrative cellular metabolomic study reveals downregulated tricarboxylic acid cycle and potential biomarkers induced by tetrabromobisphenol A in human lung A549 cells. Environ Toxicol 38 (1), 7–16.
[59] Fasulo, S., Maisano, M., Sperone, E., Mauceri, A., Bernabò, I., Cappello, T., et al., 2012. Toxicity of Foroozan crude oil to ornate wrasse (*Thalassoma pavo*, Osteichthyes, Labridae): Ultrastructure and cellular biomarkers. It J Zool 79 (2), 182–199.
[60] Demirbağ, B., Büyükafşar, K., Kaya, H., Yildirim, M., Bucak, Ö., Ünver, H., et al., 2024. Investigation of the anticancer effect of newly synthesized palladium conjugate Schiff base metal complexes on non-small cell lung cancer cell line and mouse embryonic fibroblast cell line. Biochem Biophys Res Commun 735, 150658.